ACS APPLIED MATERIALS & INTERFACES

www.acsami.org

Research Article

Highly Sensitive Photoelectrochemical Biosensor Based on Quantum Dots Sensitizing Bi_2Te_3 Nanosheets and DNA-Amplifying Strategies

Yali Yuan,* Tao Hu, Xia Zhong, Minghui Zhu, Yaqin Chai, and Ruo Yuan*

Cite This: *ACS Appl. Mater. Interfaces* 2020, 12, 22624–22629

Read Online

ACCESS | Metrics & More | Article Recommendations | Supporting Information

ABSTRACT: In this work, Bi_2Te_3 nanosheets treated with *N*-vinyl-pyrrolidinone showed highly sufficient and stable photocurrent for being used as a novel photoactive material. Accordingly, with CdTe quantum dots (QDs) sensitizing Bi_2Te_3 nanosheets, photoelectrochemical (PEC) biosensor coupling of DNA-amplifying strategies was constructed for sensitive miRNA-21 detection. Initially, the Bi_2Te_3 nanosheets on the electrode have conductive surface states with dissipationless electronic property, thus providing a highly stable photocurrent and a large surface-to-volume ratio. Then, with the participation of target miRNA-21 and auxiliary DNA, strand displacement amplification took place, thereby opening substantial DNA hairpins for triggering the next hybridization chain reaction (HCR). Through the HCR, long DNA tails decorated with CdTe QDs could thus be assembled on the electrode for enhancing the photocurrent of Bi_2Te_3 nanosheets. As a result, the proposed PEC biosensor showed a wide detection range from 10 fM to 100 pM with a detection limit of 3.3 fM, displaying a promising avenue to construct simple, ultrasensitive, and stable analytical techniques and tremendous potential in bioanalysis and early clinical diagnosis.

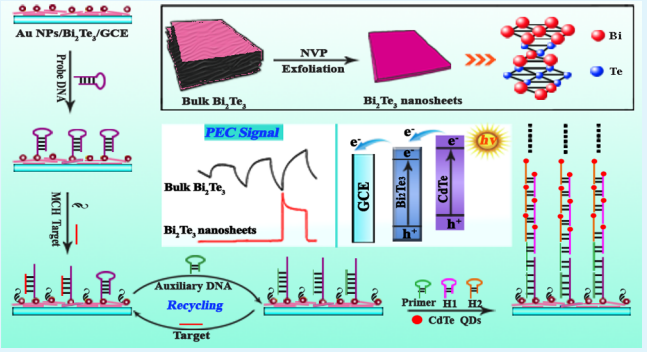

KEYWORDS: *Bi_2Te_3 nanosheets, CdTe quantum dots, photoelectrochemical biosensor, DNA amplifying strategies, sensitive detection*

1. INTRODUCTION

Photoelectrochemical (PEC) bioassay as a thriving analytical technique displays the merits of sensitive response, stable signal intensity, and time-saving operation.[1−6] Generally, PEC assay monitors and reflects the photoinduced current signal in real time; therefore, the photoactive material that generates photocurrent plays an important role in promotion of analysis performance of PEC systems.[7−9] Up to now, various photoactive materials such as TiO_2,[10−12] fullerene,[13,14] BiOI,[15,16] and graphene[17] have been extensively investigated in the fabrication of PEC biosensors. Although encouraging effects in PEC signal output were achieved, limited light absorption or the gapless nature may impede their widespread applications.[18] Therefore, there is still a need to find more advanced photoactive materials with desirable optoelectronic properties, on the basis of which new sensing PEC assay systems can be readily developed.

Bi_2Te_3, an emerging topological insulator layered material, has attracted massive interest because of its glamorous electronic properties.[19,20] As a typical topological insulator, Bi_2Te_3 possesses conductive surface states which could permit dissipationless electric conduction at room temperature, that is, the flow of electrons on its surface is topologically protected against backscattering from defects and impurities, thus being mainly applied in thermoelectric devices. On the other hand, being a layered material, Bi_2Te_3 simultaneously is a two-dimensional system with high specific surface areas and unprecedented optoelectronic properties that are important for sensing, catalysis, and energy exchange.[21−24] However, the nanosheets of layered Bi_2Te_3 commonly stack into three-dimensional crystals through van der Waals interactions. Therefore, approaches should be developed to exfoliate layered materials in order to produce mono-, double-, and few-layer crystals. More importantly, it has been reported that some bulk-layered materials are indirect band gap semiconductors, while their few-layer crystals feature a direct band gap and simultaneously, the band gap gradually increases with decreasing thickness.[25] The aforementioned optoelectronic properties of Bi_2Te_3 make it potentially intriguing in PEC assays.

Received: March 10, 2020
Accepted: April 24, 2020
Published: April 24, 2020

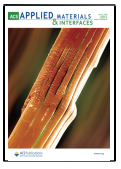

https://dx.doi.org/10.1021/acsami.0c04536
ACS Appl. Mater. Interfaces 2020, 12, 22624–22629

Scheme 1. Schematic Illustration of (A) Synthesis of Bi_2Te_3 Nanosheets, (B) Assembly Process of the PEC Biosensor, and (C) Mechanism of Photocurrent Generation

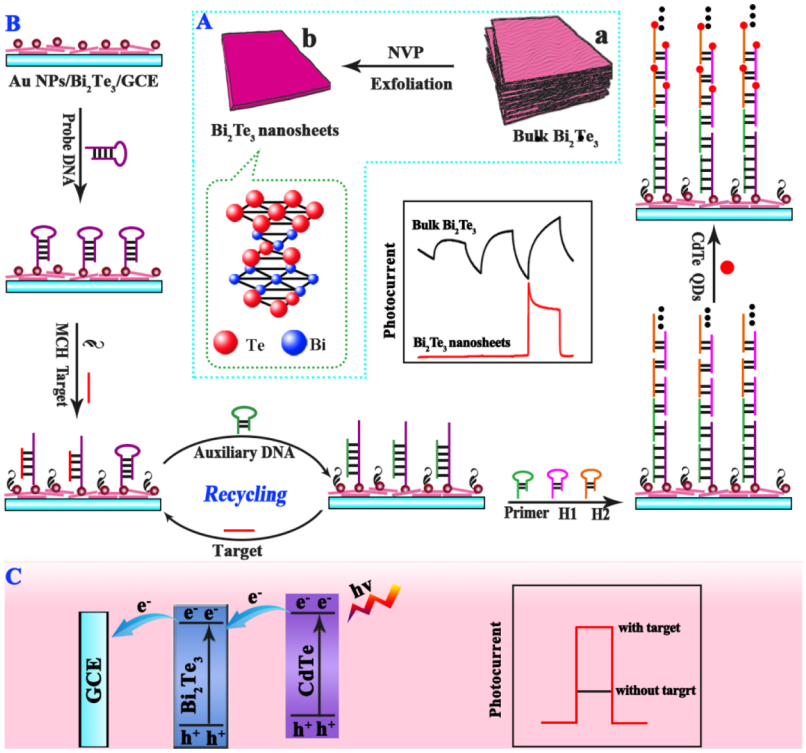

In this work, the succinct synthesis and subsequent exfoliation of bulk Bi_2Te_3 crystals in *N*-vinyl-pyrrolidinone (NVP) solvent were accomplished to give few-layer Bi_2Te_3 crystals, providing excellent surface areas for delivering free electrons and a rational band gap for light absorption. The mild surfactant polyvinylpyrrolidone was insensitive to air or water and would peel off bulk Bi_2Te_3 into few-layer crystals, ensuring a desirable direct band gap for generating sufficient and stable PEC signals under illumination. Besides that, the exfoliated Bi_2Te_3 nanosheets were found to exhibit a relatively uniform and rational light absorption range and forbidden band gap. In this case, Bi_2Te_3 nanosheets as the novel photoactive material can be beneficial for the construction of PEC biosensors.

As depicted in Scheme 1, with Bi_2Te_3 nanosheets as the photoactive material and CdTe quantum dots (QDs) as the sensitizer, for the first time, a PEC biosensor was constructed for sensitive detection of miRNA-21 by coupling of DNA-amplifying strategies. Initially, pre-exfoliated few-layer Bi_2Te_3 nanosheets were dropped on an electrode and subsequently electrodeposited with gold nanoparticles (AuNPs). Afterward, a hairpin DNA probe was immobilized on the electrode, thus initiating the hybridization chain reaction (HCR) in response to circulation of the target and auxiliary DNA probe, thereby generating substantial long DNA tails to load CdTe QDs using a cross-linker. Herein, the CdTe QDs could not only broaden the absorption of solar light for significantly reducing the destructive effect of UV light but also match the energy level of Bi_2Te_3 to facilitate charge separation, thereby effectively amplifying the photocurrent response of Bi_2Te_3 by the sensitizing effect of CdTe QDs. The proposed PEC biosensor is convenient, efficient, and thus shows considerable promise for disease diagnosis and clinical analysis.

2. EXPERIMENTAL SECTION

2.1. Preparation of Bi_2Te_3 Nanosheets. In the typical procedure for synthesis of bulk Bi_2Te_3 crystals,[26] 2 mM EDTA, 0.5 mM $BiCl_3$, and 0.8 mM Na_2TeO_3 were dissolved in 40 mL of deionized water, accompanied by the adjustment of pH to 11 by utilizing 1 M NaOH solution. Then, 30 mM $NaBH_4$ was added to the mixture and stirred for several minutes. Afterward, the solution prepared above was transferred into a Teflon-lined stainless-steel autoclave with a capacity of 50 mL. After being sealed and maintained at 200 °C for 24 h, the autoclave was allowed to cool in air. The black product thereby obtained had a high yield of about 80%. Thereafter, Bi_2Te_3 nanosheets were obtained *via* liquid exfoliation of bulk Bi_2Te_3 crystals. Briefly, a portion of 100 mg of bulk Bi_2Te_3 crystals was exfoliated in 100 mL of aqueous dispersion containing 20 μL of NVP at room temperature for 48 h, resulting in a dark grey dispersion. Subsequently, the supernatant was collected for further experiments.

2.2. Synthesis of CdTe QDs. For the synthesis of carboxy-modified CdTe QDs,[27−30] 1 mM $CdCl_2$ and 2 mM 3-mercaptopropionic acid (MPA) were added into 100 mL of aqueous solution, accompanied by the adjustment of pH to 12 by the addition of 1.0 M NaOH. After being deoxygenated with N_2 for 10 min, the solution was mixed successively with 5 mM $NaBH_4$ and 0.5 mM Na_2TeO_3 under stirring. The molar ratio of Cd^{2+}/Te^{2-}/MPA was 1:0.5:2. Then, the solution was transferred in a three-necked flask and refluxed at 100 °C for 6 h. The carboxy-modified CdTe QDs were thus collected and washed with deionized water and ethanol. Prior to modification, the carboxyl groups on the CdTe QDs need to be activated using EDC and NHS, aiming at binding with amino-functionalized H_1 and H_2 DNA.

2.3. Fabrication of Bi_2Te_3 Nanosheets and a DNA Amplification-Based PEC Biosensor. After being entirely burnished and ultrasonically rinsed, a glassy carbon electrode (GCE) was coated with 20 μL of Bi_2Te_3 nanosheets, followed by electrodepositing a layer of AuNPs. Then, 20 μL of 2.5 μM hairpin DNA probe (probe DNA) was immobilized on the electrode for an incubation time of 12 h at 4 °C. Subsequently, 10 μL of 0.3 μM blocking reagent 6-mercaptohexanol (MCH) was dropped on the

https://dx.doi.org/10.1021/acsami.0c04536
ACS Appl. Mater. Interfaces 2020, 12, 22624−22629

electrode. The obtained electrode was then applied as the PEC biosensor and thus subjected to a mixture containing 10 μL of target miRNA-21 with various concentrations and 10 μL of 2.5 μM auxiliary DNA probe for an incubation time of 45 min. During this reaction, the miRNA-21 hybridized with probe DNA and opened the hairpin structure, while the auxiliary DNA probe displaced the miRNA-21 to complete the strand displacement amplification process. Then, 20 μL of a mixture containing 2.5 μM hairpin DNA primer (trigger DNA), H_1, and H_2 was dropped on the electrode with an incubation period of 60 min for the HCR process. Finally, 20 μL of activated CdTe QDs was decorated on the electrode with an incubation period of 100 min.

3. RESULTS AND DISCUSSION

3.1. Morphology Characterizations of Bi_2Te_3. To characterize the morphologies of bulk and Bi_2Te_3 nanosheet crystals, scanning electron microscopy (SEM) and transmission electron microscopy (TEM) were employed, respectively. The SEM image in Figure 1A shows that the prepared

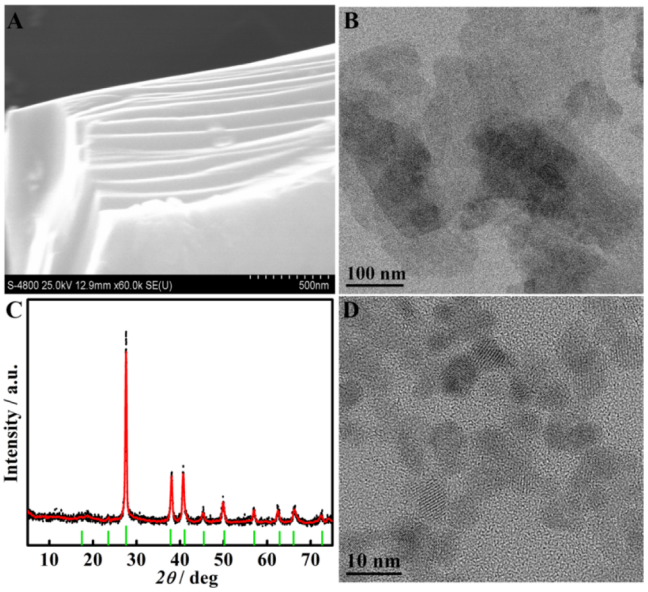

Figure 1. Characterizations of materials: SEM (A) and XRD (C) analyses of the bulk Bi_2Te_3. TEM (B,D) analyses of the Bi_2Te_3 nanosheets and CdTe QDs, respectively.

bulk Bi_2Te_3 crystals possessed a distinct multilayer stacked structure. After the liquid exfoliation of bulk Bi_2Te_3 crystals to form the Bi_2Te_3 nanosheets, some thin flakes were observed in Figure 1B with the usage of the TEM technique.

Moreover, XRD characterization was employed to identify the phase purity and crystal structure of the bulk Bi_2Te_3. As shown in Figure 1C, all of the detected peaks (red line) were consistent with those of the Bi_2Te_3 crystal structure (green line, JCPDS no. 82-0358), suggesting the successful synthesis of Bi_2Te_3 crystals. In addition, no interference peaks were observed in the XRD pattern, which further confirmed that the obtained Bi_2Te_3 crystals possessed high purity. Additionally, the TEM analysis of CdTe QDs is displayed in Figure 1D. It can be observed that the majority of prepared QDs possess a diameter of 5 nm.

3.2. Optical Properties of Bi_2Te_3 Nanosheets. The light absorption property of Bi_2Te_3 nanosheets was investigated using a UV−vis spectrometer and the result is shown in Figure 2A. It could be observed that the Bi_2Te_3 nanosheets exhibited strong absorption in the visible light region. The optical data

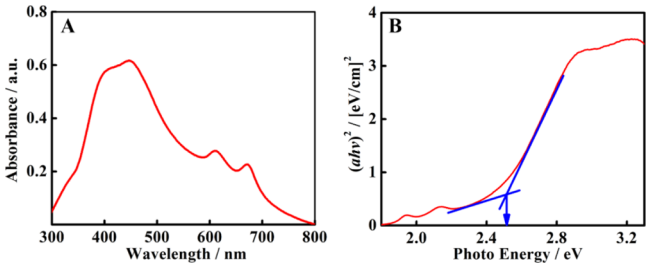

Figure 2. Light absorption curve (A) and Tauc plot (B) of the synthesized Bi_2Te_3 nanosheets.

were analyzed using the classical absorption equation $\alpha = a(h\nu - E_g)^{1/r}/h\nu$, where "$\alpha$" is the molar absorption coefficient, "a" is a constant, "$h\nu$" is the photon energy, "E_g" is the optical band gap value, and the value of the exponent "r" denoted the nature of the transition, allowing direct transition (r = 1/2) and indirect transition (r = 2). Then, the Tauc plot that showed the quantity $h\nu$ on the abscissa and the quantity $(\alpha h\nu)^{1/r}$ on the ordinate were used to determine the optical band gap value of the Bi_2Te_3 nanosheets. As displayed in Figure 2B, a distinct linear regime was obtained. The tangency point of the linear region to the abscissa had a value of 2.52 eV for the optical band gap.

3.3. Cyclic Voltammetry and Electrochemical Impedance Spectroscopy Measurements. For the purpose of stepwise characterizing the modified electrode, both cyclic voltammetry (CV) and electrochemical impedance spectroscopy (EIS) techniques were employed here. Figure 3A displays

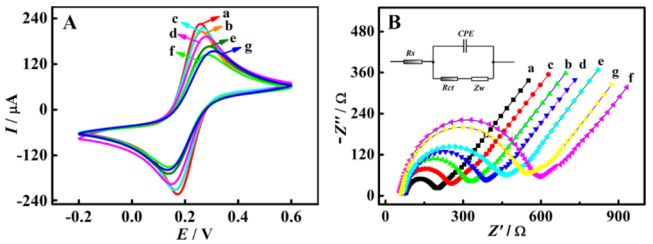

Figure 3. Stepwise CV (A) and EIS (B) analysis of the fabricated PEC biosensor: (a) GCE, (b) Bi_2Te_3/GCE, (c) AuNPs/Bi_2Te_3/GCE, (d) DNA probe/AuNPs/Bi_2Te_3/GCE, (e) MCH/DNA probe/AuNPs/Bi_2Te_3/GCE, (f) nanowire/MCH/DNA probe/AuNPs/Bi_2Te_3/GCE, and (g) CdTe/nanowire/MCH/DNAprobe/AuNPs/Bi_2Te_3/GCE in $[Fe(CN)_6]^{3-/4-}$.

the CV results of different modified electrodes. The bare electrode showed an explicit redox peak of $[Fe(CN)_6]^{3-/4-}$ (curve a). After modifying Bi_2Te_3 nanosheets on the GCE, the redox peak obviously decreased (curve b). When electrodepositing the AuNPs, the electrode displayed an increased redox peak owing to its conductivity (curve c). Afterward, the assembly of the DNA probe on AuNPs/Bi_2Te_3/GCE decreased the redox peak (curve d), attributing to the electronic repulsion of electronegative $[Fe(CN)_6]^{3-/4-}$. Moreover, the redox peaks continued to decrease after the assembly of inert MCH (curve e) and HCR products of the DNA nanowire (curve f). However, the redox peak increased after the decoration of CdTe QDs on the DNA nanowire (curve g).

Moreover, EIS was also used for investigating the stepwise modified process of the proposed biosensor. The results are shown in Figure 3B. The bare GCE had a small R_{et} value (curve a). Afterward, the R_{et} value increased with modification

https://dx.doi.org/10.1021/acsami.0c04536
ACS Appl. Mater. Interfaces 2020, 12, 22624−22629

of semiconductor Bi_2Te_3 nanosheets (curve b). Afterward, further immobilization of AuNPs acquired a decreased R_{et} value (curve c). Because the DNA and MCH inherited the inert property, there appeared an ongoing increase in the R_{et} value after the successive assembly of the DNA probe (curve d), MCH (curve e), and DNA nanowire (curve f). Nevertheless, the R_{et} value decreased after the modification of conductive CdTe QDs (curve g). In all, the results of EIS were consistent with those of CV measurement.

3.4. Analytical Performance of the Proposed PEC Biosensor. To examine the quantitative performance of the constructed biosensor, the correlation between PEC response and concentration of miRNA-21 was investigated under optimized conditions. As depicted in Figure 4A, the PEC

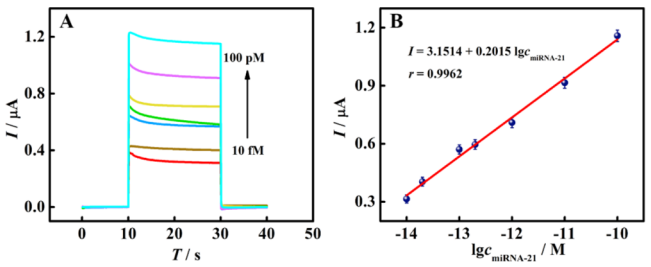

Figure 4. (A) PEC signals for various concentrations of miRNA-21 (10 fM, 20 fM, 100 fM, 200 fM, 1 pM, 10 pM, and 100 pM) and (B) corresponding linear relationship between the photocurrent and logarithm of miRNA-21 concentration (n = 3).

signals *versus* different concentrations of miRNA-21 increased gradually with increasing concentration of miRNA-21 in the range of 10 fM to 100 pM. As shown in Figure 4B, the linear equation was calculated to be $I = 3.1541 + 0.2015 \lg c$, where I indicates the photocurrent of the biosensor and c refers to the target concentration. The calculative limit of detection was 3.3 fM on the basis of the expression S/N = 3. Moreover, the performance comparison of different biosensors for miRNA-21 detection is displayed in Table S2. The results showed that the biosensor presented a prominent application in sensitive detection of miRNA-21 owing to the Bi_2Te_3−CdTe-sensitizing system and DNA-amplifying strategies.

3.5. Specificity and Stability of the Proposed PEC Biosensor. Selectivity is an essential performance indicator of the PEC assay and represents its potentiality in practical application or clinical research. As shown in Figure 5A, the photocurrent caused by 1 nM of interferences was akin to that of the blank control and was drastically different from the

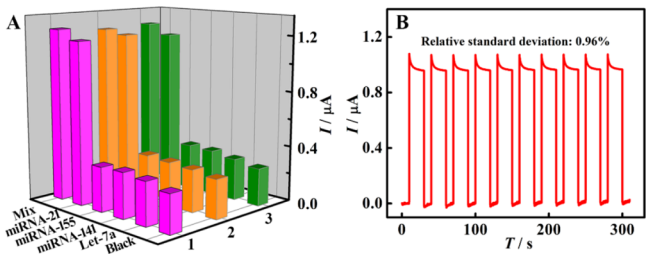

Figure 5. (A) Specificity of the biosensor toward the blank control, let-7a (1 nM), miRNA-141 (1 nM), miRNA-155 (1 nM), miRNA-21 (100 pM), and the mixture (100 pM miRNA-21 with 1 nM let-7a, microRNA-141, and miRNA-155) and (B) stability of the biosensor under consecutive off−on−off illumination for 10 cycles.

response caused by 100 pM miRNA-21, illustrating the excellent specificity of the designed biosensor owing to the specific recognition between the DNA probe and target miRNA-21. Furthermore, Figure 5B exhibits the desirable stability of the proposed biosensor under successive on−off−on illumination for 10 circulations at 10 pM miRNA-21.

3.6. Practical Application of the PEC Biosensor. Here, the analysis of lysates from HeLa and MCF-7 cells was adopted to appraise the practicability of the proposed PEC assay. The corresponding photocurrents of the successively enlarged amount (from 1×10^3 to 500×10^3) of HeLa and CEF-7 cells were measured and recorded. Results in Figure 6 show

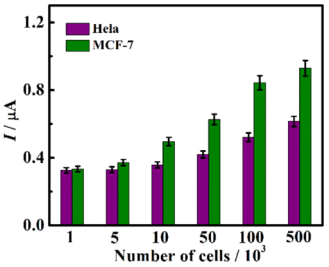

Figure 6. PEC signals of the proposed biosensor incubated with HeLa and MCF-7 cells (n = 3).

that miRNA-21 exists more in MCF-7 cells and less in HeLa cells, analogous to previously published literature.[31,32] Therefore, it indicated that the PEC biosensor might achieve feasible results for clinical research.

4. CONCLUSIONS

In summary, by coupling of DNA-amplifying strategies, a novel PEC biosensor based on the Bi_2Te_3−CdTe photoelectric conversion and enhancement system was prepared for highly sensitive miRNA-21 detection. The Bi_2Te_3 nanosheets featured not only more active edge sites but also a direct band gap, providing a sufficient and stable photocurrent signal for PEC analysis. In addition, the HCR strategy based on the strand displacement amplification (SDR) further improved the analytical performance of the biosensor. *In vitro* assays and cell lysates demonstrated that the proposed biosensor showed a prominent analytical performance for miRNA-21, showing tremendous potential in bioanalysis and early clinical diagnosis.

■ ASSOCIATED CONTENT

Supporting Information

The Supporting Information is available free of charge at https://pubs.acs.org/doi/10.1021/acsami.0c04536.

Experimental details for the used chemicals and materials, apparatus, electrochemical measurement, PAGE characterization of the proposed strategy, optimal conditions for the prepared biosensor, and comparison of different biosensors (PDF)

■ AUTHOR INFORMATION

Corresponding Authors

Yali Yuan − *Chongqing Engineering Laboratory of Nanomaterials & Sensor Technologies, College of Chemistry and Chemical Engineering, Southwest University, Chongqing 400715, China*; Email: y198688@swu.edu.cn

https://dx.doi.org/10.1021/acsami.0c04536
ACS Appl. Mater. Interfaces 2020, 12, 22624−22629

Ruo Yuan − *Chongqing Engineering Laboratory of Nanomaterials & Sensor Technologies, College of Chemistry and Chemical Engineering, Southwest University, Chongqing 400715, China;* orcid.org/0000-0003-3664-6236; Email: yuanruo@swu.edu.cn

Authors

Tao Hu − *Chongqing Engineering Laboratory of Nanomaterials & Sensor Technologies, College of Chemistry and Chemical Engineering, Southwest University, Chongqing 400715, China*

Xia Zhong − *Chongqing Engineering Laboratory of Nanomaterials & Sensor Technologies, College of Chemistry and Chemical Engineering, Southwest University, Chongqing 400715, China*

Minghui Zhu − *Chongqing Engineering Laboratory of Nanomaterials & Sensor Technologies, College of Chemistry and Chemical Engineering, Southwest University, Chongqing 400715, China*

Yaqin Chai − *Chongqing Engineering Laboratory of Nanomaterials & Sensor Technologies, College of Chemistry and Chemical Engineering, Southwest University, Chongqing 400715, China;* orcid.org/0000-0003-4392-9592

Complete contact information is available at: https://pubs.acs.org/10.1021/acsami.0c04536

Notes

The authors declare no competing financial interest.

■ ACKNOWLEDGMENTS

This work was supported by the Fundamental Research Funds for the Central Universities (XDJK2020TY002, XDJK2019B022, XDJK2018C041) and the National Natural Science Foundation (NNSF) of China (51473136, 21575116).

■ REFERENCES

(1) Zhao, W.-W.; Xu, J.-J.; Chen, H.-Y. Photoelectrochemical Bioanalysis: the State of the Art. *Chem. Soc. Rev.* **2015**, *44*, 729−741.

(2) Deng, H.-M.; Zhu, M.-H.; Huang, L.-J.; Chai, Y.-Q.; Liu, X.-R.; Yuan, R.; Yuan, Y.-L. Novel D-A-D-Type Supramolecular Aggregates with High Photoelectric Activity for Construction of Ultrasensitive Photoelectrochemical Biosensor. *Anal. Chem.* **2019**, *91*, 12468−12475.

(3) Li, P.-P.; Cao, Y.; Mao, C.-J.; Jin, B.-K.; Zhu, J.-J. TiO_2/g-C_3N_4/CdS Nanocomposite-Based Photoelectrochemical Biosensor for Ultrasensitive Evaluation of T4 Polynucleotide Kinase Activity. *Anal. Chem.* **2019**, *91*, 1563−1570.

(4) Chu, Y.; Deng, A.-P.; Wang, W.; Zhu, J.-J. Concatenated Catalytic Hairpin Assembly/Hyperbranched Hybridization Chain Reaction Based Enzyme-Free Signal Amplification for the Sensitive Photoelectrochemical Detection of Human Telomerase RNA. *Anal. Chem.* **2019**, *91*, 3619−3627.

(5) Wang, C.; Li, Y.; Xu, E.; Zhou, Q.; Chen, J.; Wei, W.; Liu, Y.; Liu, S. A Label-free PFP-based Photoelectrochemical Biosensor for Highly Sensitive Detection of PARP-1 Activity. *Biosens. Bioelectron.* **2019**, *138*, 111308.

(6) Zhu, M.; Zhong, X.; Deng, H.; Huang, L.; Yuan, R.; Yuan, Y. Dependent Signal Quenching and Enhancing Triggered by Bipedal DNA Walker for Ultrasensitive Photoelectrochemical Biosensor. *Biosens. Bioelectron.* **2019**, *143*, 111618.

(7) Lewis, N. S. Research Opportunities to Advance Solar Energy Utilization. *Science* **2016**, *351*, aad1920.

(8) Li, J.; Wu, N. Semiconductor-based Photocatalysts and Photoelectrochemical Cells for Solar Fuel Generation: A Review. *Catal. Sci. Technol.* **2015**, *5*, 1360−1384.

(9) Huang, L.; Deng, H.; Zhong, X.; Zhu, M.; Chai, Y.; Yuan, R.; Yuan, Y. Wavelength Distinguishable Signal Quenching and Enhancing Toward Photoactive Material 3,4,9,10-perylenetetracarboxylic Dianhydride for Simultaneous Assay of Dual Metal Ions. *Biosens. Bioelectron.* **2019**, *145*, 111702−111707.

(10) Wang, M.; Yin, H.; Zhou, Y.; Sui, C.; Wang, Y.; Meng, X.; Waterhouse, G. I. N.; Ai, S. Photoelectrochemical Biosensor for MicroRNA Detection Based on a MoS_2/g-C_3N_4/black TiO_2 Heterojunction with Histostar@AuNPs for Signal Amplification. *Biosens. Bioelectron.* **2019**, *128*, 137−143.

(11) Liu, P. P.; Liu, X.; Huo, X. H.; Tang, Y.; Xu, J.; Ju, H. TiO_2−$BiVO_4$ Heterostructure to Enhance Photoelectrochemical Efficiency for Sensitive Aptasensing. *ACS Appl. Mater. Interfaces* **2017**, *9*, 27185−27192.

(12) Dai, H.; Zhang, S.; Hong, Z.; Lin, Y. A Potentiometric Addressable Photoelectrochemical Biosensor for Sensitive Detection of Two Biomarkers. *Anal. Chem.* **2016**, *88*, 9532−9538.

(13) Zheng, Y.-N.; Liang, W.-B.; Xiong, C.-Y.; Yuan, Y.-L.; Chai, Y.-Q.; Yuan, R. Self-Enhanced Ultrasensitive Photoelectrochemical Biosensor Based on Nanocapsule Packaging Both Donor−Acceptor-Type Photoactive Material and Its Sensitizer. *Anal. Chem.* **2016**, *88*, 8698−8705.

(14) Long, D.; Li, M.; Wang, H.; Wang, H.; Chai, Y.; Yuan, R. A Photoelectrochemical Biosensor Based on Fullerene with Methylene Blue as a Sensitizer for Ultrasensitive DNA Detection. *Biosens. Bioelectron.* **2019**, *142*, 111579.

(15) Han, Q.; Wang, R.; Xing, B.; Zhang, T.; Khan, M. S.; Wu, D.; Wei, Q. Label-free Photoelectrochemical Immunoassay for CEA Detection Based on CdS Sensitized WO_3@BiOI Heterostructure Nanocomposite. *Biosens. Bioelectron.* **2018**, *99*, 493−499.

(16) Zhu, Y.; Yan, K.; Xu, Z.; Wu, J.; Zhang, J. Cathodic "Signal-on" Photoelectrochemical Aptasensor for Chloramphenicol Detection Using Hierarchical Porous Flower-like Bi-BiOI@C Composite. *Biosens. Bioelectron.* **2019**, *131*, 79−87.

(17) Cai, G.; Yu, Z.; Ren, R.; Tang, D. Exciton−Plasmon Interaction between AuNPs/Graphene Nanohybrids and CdS Quantum Dots/TiO_2 for Photoelectrochemical Aptasensing of Prostate-Specific Antigen. *ACS Sens.* **2018**, *3*, 632−639.

(18) Zhong, M.; Hisatomi, T.; Kuang, Y.; Zhao, J.; Liu, M.; Iwase, A.; Jia, Q.; Nishiyama, H.; Minegishi, T.; Nakabayashi, M.; Shibata, N.; Niishiro, R.; Katayama, C.; Shibano, H.; Katayama, M.; Kudo, A.; Yamada, T.; Domen, K. Surface Modification of CoOx Loaded $BiVO_4$ Photoanodes with Ultrathin p-Type NiO Layers for Improved Solar Water Oxidation. *J. Am. Chem. Soc.* **2015**, *137*, 5053−5060.

(19) Kim, C.; Yang, Y.; Baek, J. Y.; Lopez, D. H.; Kim, D. H.; Kim, H. Concurrent Defects of Intrinsic Tellurium and Extrinsic Silver in an n-type $Bi_2Te_{2.88}Se_{0.15}$ Thermoelectric Material. *Nano Energy* **2019**, *60*, 26−35.

(20) Choi, H.; Jeong, K.; Chae, J.; Park, H.; Baeck, J.; Kim, T. H.; Song, J. Y.; Park, J.; Jeong, K.-H.; Cho, M.-H. Enhancement in Thermoelectric Properties of Te-embedded Bi_2Te_3 by Preferential Phonon Scattering in Heterostructure Interface. *Nano Energy* **2018**, *47*, 374−384.

(21) Shi, Y.; Zhang, B. Recent Advances in Transition Metal Phosphide Nanomaterials: Synthesis and Applications in Hydrogen Evolution Reaction. *Chem. Soc. Rev.* **2016**, *45*, 1529−1541.

(22) Luo, B.; Liu, G.; Wang, L. Recent Advances in 2D Materials for Photocatalysis. *Nanoscale* **2016**, *8*, 6904−6920.

(23) Nicolosi, V.; Chhowalla, M.; Kanatzidis, M. G.; Strano, M. S.; Coleman, J. N. Liquid Exfoliation of Layered Materials. *Science* **2013**, *340*, 1226419.

(24) Coleman, J. N.; Lotya, M.; O'Neill, A.; Bergin, S. D.; King, P. J.; Khan, U.; Young, K.; Gaucher, A.; De, S.; Smith, R. J.; Shvets, I. V.; Arora, S. K.; Stanton, G.; Kim, H.-Y.; Lee, K.; Kim, G. T.; Duesberg, G. S.; Hallam, T.; Boland, J. J.; Wang, J. J.; Donegan, J. F.; Grunlan, J. C.; Moriarty, G.; Shmeliov, A.; Nicholls, R. J.; Perkins, J. M.; Grieveson, E. M.; Theuwissen, K.; McComb, D. W.; Nellist, P. D.; Nicolosi, V. Two-Dimensional Nanosheets Produced by Liquid Exfoliation of Layered Materials. *Science* **2011**, *331*, 568.

(25) Eda, G.; Yamaguchi, H.; Voiry, D.; Fujita, T.; Chen, M.; Chhowalla, M. Photoluminescence from Chemically Exfoliated MoS2. *Nano Lett.* **2011**, *11*, 5111−5116.
(26) Mi, J.-L.; Lock, N.; Sun, T.; Christensen, M.; Søndergaard, M.; Hald, P.; Hng, H. H.; Ma, J.; Iversen, B. B. Biomolecule-Assisted Hydrothermal Synthesis and Self-Assembly of Bi2Te3 Nanostring-Cluster Hierarchical Structure. *ACS Nano* **2010**, *4*, 2523−2530.
(27) Sun, B.; Dong, J.; Cui, L.; Feng, T.; Zhu, J.; Liu, X.; Ai, S. A Dual Signal-on Photoelectrochemical Immunosensor for Sensitively Detecting Target Avian Viruses Based on AuNPs/g-C_3N_4 Coupling with CdTe Quantum Dots and in Situ Enzymatic Generation of Electron Donor. *Biosens. Bioelectron.* **2019**, *124−125*, 1−7.
(28) Zhu, H.-Y.; Ding, S.-N. Dual-signal-amplified Electrochemiluminescence Biosensor for MicroRNA Detection by Coupling Cyclic Enzyme with CdTe QDs Aggregate as Luminophor. *Biosens. Bioelectron.* **2019**, *134*, 109−116.
(29) Vaishnav, J. K.; Mukherjee, T. K. Surfactant-Induced Self-Assembly of CdTe Quantum Dots into Multicolor Luminescent Hybrid Vesicles. *Langmuir* **2019**, *35*, 6409−6420.
(30) Jie, G.; Li, C.; Zhao, Y.; Kuang, Q.; Niu, S. Fluorescent Mn:ZnCdS@ZnS and CdTe Quantum Dots Probes on SiO_2 Microspheres for Versatile Detection of Carcinoembryonic Antigen and Monitoring T4 Polynucleotide Kinase Activity. *ACS Appl. Nano Mater.* **2019**, *2*, 4637−4645.
(31) Ye, S.; Li, X.; Wang, M.; Tang, B. Fluorescence and SERS Imaging for the Simultaneous Absolute Quantification of Multiple miRNAs in Living Cells. *Anal. Chem.* **2017**, *89*, 5124−5130.
(32) Si, M.-L.; Zhu, S.; Wu, H.; Lu, Z.; Wu, F.; Mo, Y.-Y. MiR-21-Mediated Tumor Growth. *Oncogene* **2007**, *26*, 2799−2803.

https://dx.doi.org/10.1021/acsami.0c04536
ACS Appl. Mater. Interfaces 2020, 12, 22624−22629